COMPDYN 2023
9th ECCOMAS Thematic Conference on
Computational Methods in Structural Dynamics and Earthquake Engineering
M. Papadrakakis, M. Fragiadakis (eds.)
Athens, Greece, 12-14 June 2023

FRAGILITY FUNCTION UNCERTAINTY QUANTIFICATION IN INFILLED RC FRAME BUILDINGS

Al Mouayed Bellah Nafeh[1], **Gerard J. O'Reilly**[1]

[1] Centre for Training and Research on Reduction of Seismic Risk (ROSE Centre) Scuola Universitaria Superiore IUSS Pavia
Palazzo del Broletto, Piazza della Vittoria 15, Pavia 27100, Italy
e-mail: {mouayed.nafeh, gerard.oreilly}@iusspavia.it

Abstract

Seismic performance assessment within modern performance-based earthquake engineering quantifies the exceedance of a structural performance level related to a structural demand level, quantified via an engineering demand parameter (EDP). Fragility functions are used for this purpose as they represent the interface between the intensity of ground-shaking, described by an intensity measure (IM), and the probability that a damage level, or EDP threshold, is exceeded in the structure. Fragility functions are defined as a median seismic intensity required to exceed a given EDP threshold and its associated dispersion. To this end, this study aims at quantifying the dispersion in ground motion shaking intensity for a given ductility demand threshold in infilled frame buildings. The dispersions were evaluated as a function of the average spectral acceleration IM and varies with respect to the height of the considered buildings under consideration. The quantified dispersions are then implemented within a response estimation tool previously developed by the authors to refine the single-value-type dispersion previously assumed. The previous and newly defined sets of dispersion values are scrutinised within the context of fragility function estimation for a set of archetype infilled reinforced concrete frame structures and compared to the results obtained via extensive dynamic analyses, showing much improvement with no additional computational cost or complexity.

Keywords: uncertainty, fragility, intensity measure, engineering demand parameter, infilled RC

1 INTRODUCTION

Infilled reinforced concrete (RC) buildings represent a prevalent taxonomy class in the Mediterranean region. These buildings constitute a significant portion of the southern European building stock generally, and the Italian built environment specifically, as reported by the census data published by the Italian national institute of statistics (ISTAT) [1] and illustrated in Figure 1.

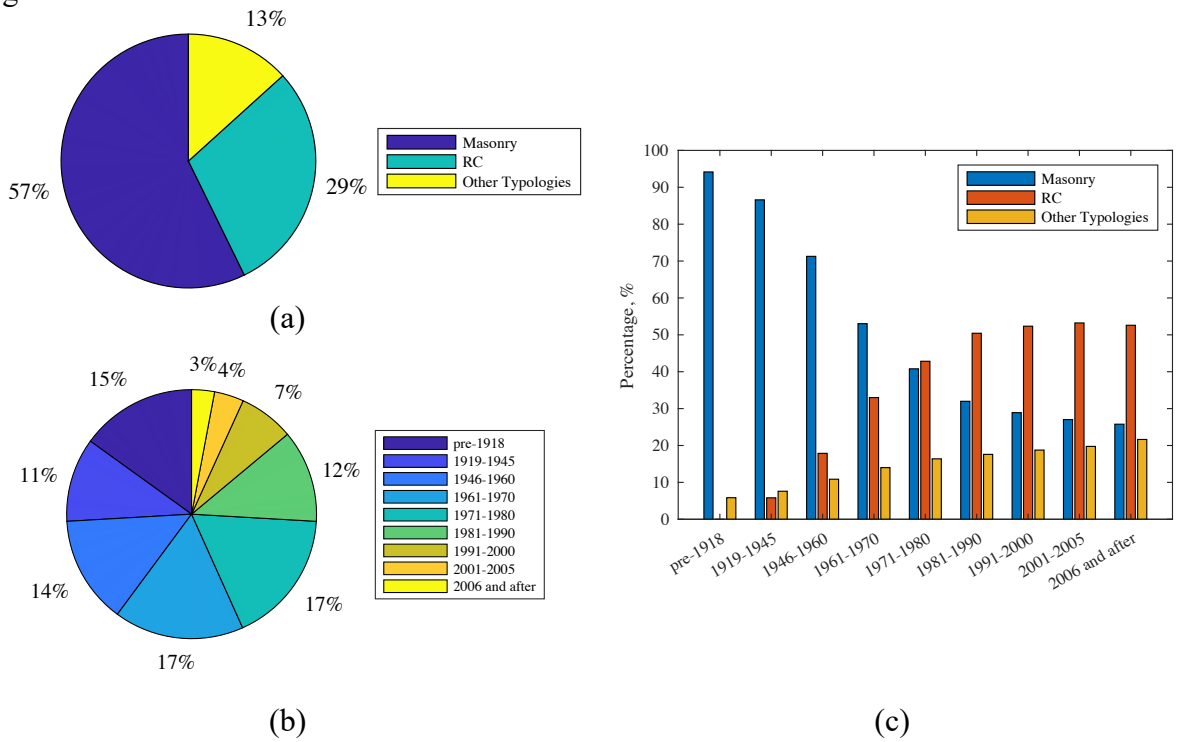

Figure 1: (a) Residential buildings by construction material; (b) RC Residential buildings by construction period; (c) Residential buildings (RC, masonry and other typologies) by construction period

RC buildings with unreinforced masonry infill panels were typically designed to resist gravity loads only or were designed before the introduction of modern seismic design guidelines (i.e., capacity-based design). The latter promotes a ductile and stable mechanism and is required by most modern-day design codes (e.g. Eurocode 8 [2] and NTC18 [3]). Before the 1970s, structural elements were designed considering gravity loads only. The allowable stress method (ASM) was used to calculate loads and the subsequent detailing of structural members. Construction features of these gravity load designed (GLD) buildings include frames spanning in one direction, the use of smooth reinforcing bars, low compressive strength concrete, rebars with low yield strengths, inadequate transverse and shear detailing, inadequate joint detailing (i.e., inadequate anchorage length and the use of end-hooks). The period between the mid-1970s and 1980s witnessed the introduction of the equivalent lateral force (ELF) method. To implement the ELF method, a seismic coefficient, defined as around 7%-10% was required [4–7]. This design methodology was coupled with ASM to size and detail structural members. Construction features of this sub-standard design (SSD) practice include frames spanning in one (or both) directions, the use of deformed rebars and concrete with moderate yield and compressive strengths, respectively, with no consideration of ductile detailing. The highlighted design considerations resulted in many instances of brittle and non-ductile mechanisms forming, mainly in the surrounding frame elements of infill panels and beam-column joints. Several past and recent earthquake reconnaissance observations [8–11] reported many occurrences of extensive damage and collapse cases in RC buildings with infills due to shear and flexural failure of

structural members. Analytical [12–15] and experimental [16–19] studies have also highlighted the detrimental effects of not considering masonry infills in the design process as these elements were considered non-structural components, and their effect on the structural response was neglected. This resulted in severe implications on the lateral load-resisting capacity of these buildings. Several instances of sudden infill panel rupture leading up to a differential stiffness (i.e., soft-storey mechanism) between storeys were recorded.

The seismic performance assessment of existing structures within modern performance-based earthquake engineering (PBEE) entails accurately quantifying the exceedance of any structural demand-based performance level. The latter is typically quantified using fragility curves which link the probability of exceeding predefined thresholds of demand quantified via an engineering demand parameter (EDP) for a given intensity measure (IM) level of ground-shaking. Fragility functions are usually the end result of extensive numerical analysis (i.e., numerical modelling of a case study structure, ground-motion selection, and non-linear dynamic analyses). Recent studies [20,21] highlighted the necessity for simplified tools to reduce the computational effort and time required by such extensive analyses. To this end, a response estimation tool (RET) was developed by Nafeh and O'Reilly [22] for the purpose of single-building vulnerability assessment of infilled RC frame structures (available here: https://github.com/gerardjoreilly/Infilled-RC-Building-Response-Estimation). Additionally, a simplified seismic risk evaluation methodology denoted *PB-Risk* was also proposed by Nafeh and O'Reilly [23], incorporating the aforementioned tool. The tool was developed based on empirically-derived ρ-μ-T relationships calibrated based on cloud analyses on single-degree-of-freedom (SDOF) oscillators with various backbone parameters representative of the infilled RC typology [21]. The derived ρ-μ-T relationship empirically relates the dynamic strength ratio, ρ of an SDOF system with a period of vibration T to the ductility demand, μ, via a simple static pushover (SPO) analysis. ρ is defined as the ratio between the average spectral acceleration and the yield spectral acceleration of the SDOF system, $\frac{Sa_{avg}}{Sa_y}$. The ρ-μ-T relationship is subsequently calculated via static response parameters, which can be obtained via a simple pushover analysis, as illustrated in Figure 2. The dispersion (i.e., the blue area in Figure 2) was initially quantified as the error in the regression corresponding to the median response, or the record-to-record variability, of the SDOF system and was fixed for all levels of demand. Conservative dispersion values were associated with the median intensities conditioned to non-collapse and collapse, which are 0.28 and 0.37, respectively. Therefore, the aim of this study is to provide the tool users with an updated set of dispersions derived from the inherent uncertainties of multi-degree-of-freedom (MDOF) systems. The newly derived sets of uncertainty values can be used for single-building vulnerability assessment applications as well as adopted for regional assessment applications where fragility functions are needed.

To this end, this study aims at quantifying the uncertainty in Sa_{avg} given the structural response parameter, which can be integrated within the RET (i.e. top displacement) or $\beta_{IM=Sa_{avg}|EDP=\Delta_{top}}$ for the derivation of fragility functions. As such, values of uncertainty were derived for low-rise (2-3 storeys) and mid-rise (4-6 storeys) buildings corresponding to two design eras: low-code or GLDs (i.e. pre-1970s) and moderate-code or SSDs (1970s-mid 1980s). The derived uncertainty values were then implemented within the RET and PB-Risk methodology for vulnerability and risk-based applications and compared to the results of extensive nonlinear time-history analyses (NLTHA).

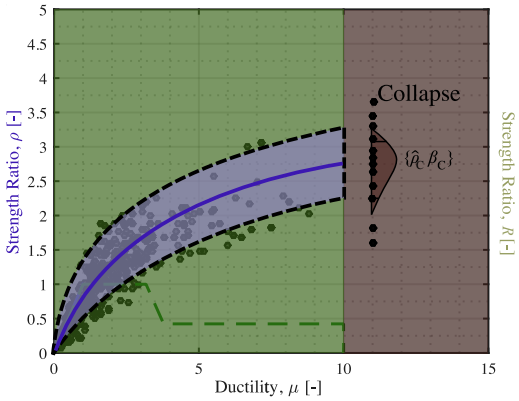

Figure 2: Example derivation of dynamic capacity curves and the collapse intensity of an SDOF system based on the static response provided via a multi linearised pushover curve.

2 QUANTIFICATION OF FRAGILITY FUNCTION UNCERTAINTY $\beta_{IM|EDP}$

A set of multiple stripe analyses (MSA) were carried out on a database of three-dimensional infilled RC archetype-building numerical models. The database includes two subsets of 35 infilled RC buildings, each designed for either gravity-loads only or the ELF method using a seismic coefficient of 10%. The numerical models were developed by Nafeh and O'Reilly [24,25] and are available at: https://github.com/gerardjoreilly/Infilled-RC-Building-Database. The archetypes were modelled in Opensees [26] using a lumped plasticity approach following the identification of key design features. The building models were sufficiently detailed to account for typical inelastic mechanisms and potential failure modes in the structure. Considering the numerical modelling, beam and column members were modelled as elastic beam-column elements with cracked section properties and zero-length elements located at a finite plastic hinge length [12,27]. Beam-column joints were modelled by adopting a scissor-type modelling approach. Adequate considerations for exterior and interior joints were adopted, reflecting on poor detailing and the use of smooth rebars with end-hooks [28,29]. Masonry infill panels were modelled using the equivalent strut approach [30], and the difference in infill strength (weak, medium and strong) were considered following the characterisation performed in Hak *et al.* [31]. An empirical calibration for strength and deformation capacities and hysteresis parameters was implemented based on experimental data for all relevant structural members presented. The adopted numerical modelling techniques and considerations are presented in detail in Nafeh & O'Reilly [22] and illustrated in Figure 3.

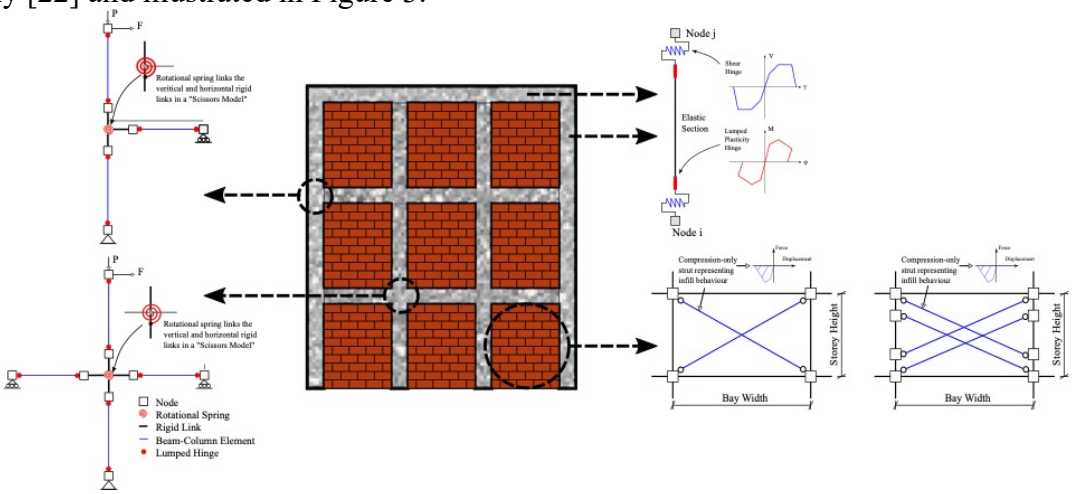

Figure 3: Numerical modelling assumptions for the infilled RC archetype numerical building models

MSA are necessary to accurately quantify the relationship between structural demand and seismic intensity. Probabilistic seismic hazard analysis (PSHA) was carried out using the OpenQuake engine [32] to characterise the site hazard adopting the average spectral acceleration [33], Sa_{avg}, as the IM given its noteworthy efficiency (i.e. low dispersion associated with the structural response) and sufficient (i.e. the estimation of demand is independent of ground-motion parameters) performance. The buildings were fictitiously located in the city of L'Aquila in central Italy, representing high seismicity. Disaggregation analysis was carried out to identify the most relevant rupture scenario(s) and allow the identification of suitable ground-motion records for MSA. Hazard-consistent records were selected from the NGA-W2 database using the EzGM tool developed by Ozsarac *et al.* [35], and the geometric mean of the two horizontal components was considered. MSA was conducted for nine-intensity measure levels spanning return periods T_R = 22 – 4975 years to characterise the structural response from initial damage right up to global structural instability or collapse. The structural response was characterised in terms of the peak storey displacement ($\boldsymbol{\Delta_i}$), which was subsequently converted to the equivalent SDOF displacement capacity (Δ_{cap}) as per Equation 1.

$$\boldsymbol{\Delta_{cap}} = \frac{\sum \boldsymbol{m_i \Delta_i^2}}{\sum \boldsymbol{m_i \Delta_i}} \tag{1}$$

Where m_i is the mass of storey *i*.

Subsequently, MSA results were expressed in terms of the IM (i.e. Sa_{avg}) and Δ_{cap} of the equivalent SDOF oscillators extracted. The seismic intensities expressed in terms of Sa_{avg} were normalised with respect to the yield spectral acceleration Sa_y to obtain the dynamic strength ratio, ρ. The ductility demand of the SDOF oscillators was derived by normalising the deformation capacity Δ_{cap} by the yield deformation Δ_y^* of each equivalent SDOF system determined as per Equation 2.

$$\Delta_y^* = \frac{\Delta_y}{\Gamma} \tag{2}$$

Where Δ_y is the yield displacement of the MDOF system; Γ is the first-mode transformation factor. An example illustration of the process is provided in Figure 4.

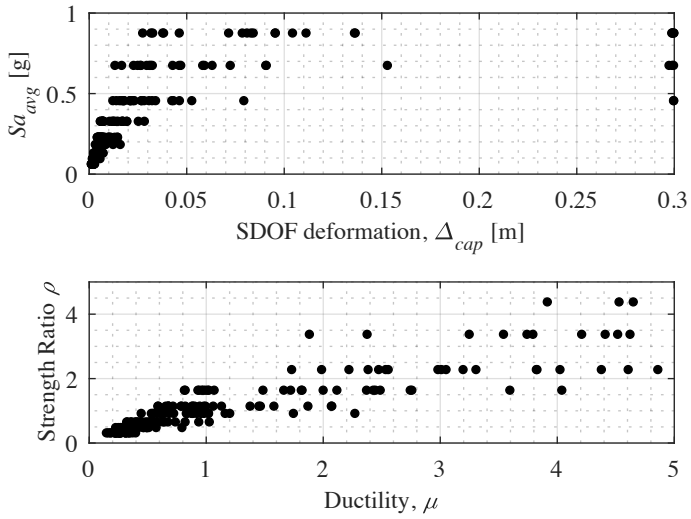

Figure 4: Example illustration of the MSA carried out on a single three-storey GLD archetype building model where the results are expressed in terms of the average spectral acceleration and the equivalent SDOF deformation capacity; and the normalised results expressed in terms of the strength ratio and ductility

MSA results were subsequently disaggregated based on two principal taxonomy characteristics, namely the number of storeys (i.e. for 2, 3, 4, 5 and 6) and the previously adopted design practice (i.e. pre-1970s GLD buildings and SSD structures designed for moderate code levels using ELF method). This resulted in the identification of four taxonomies in this study as reported in Table 1. This consideration provides more refined insight into the associated dispersions and may even be used on the regional scale of vulnerability assessment for the typology under scrutiny. Furthermore, the dispersion associated with the median intensities corresponding to a range of SDOF deformation capacities was derived by applying maximum likelihood estimation to the results of MSA for each numerical building model. The individual dispersion trends, expressed in terms of $\beta_{\rho|\mu}$ derived across the highlighted ductility range, are illustrated in Figure 5. Moreover, Figure 5 illustrates the mean and the suggested $\beta_{\rho|\mu}$ limits derived in this study as well as the $\beta_{\rho|\mu}$ limits for non-collapse and collapse considerations to previously integrated within the RET tool. Generally, it was noted that the initial dispersion limit of 0.38 associated with collapse was highly conservative for all observed cases as opposed to the newly derived values between 0.23-0.28. Additionally, for non-collapse, the previously assigned dispersion threshold of 0.28 was not very conservative; however, a reduction in uncertainty was observed for some taxonomy cases such as the mid-rise low and moderate code buildings. The advantage of calibrating a new set of dispersion limits is the reduction in the overall uncertainty corresponding with the entire range of structural response which is integrated in both vulnerability and risk-based applications. It is also a reflection on the efficiency property of the average spectral acceleration whereby the dispersion associated with higher levels of intensities causing large inelastic demands in the structure tends to be generally minimized.

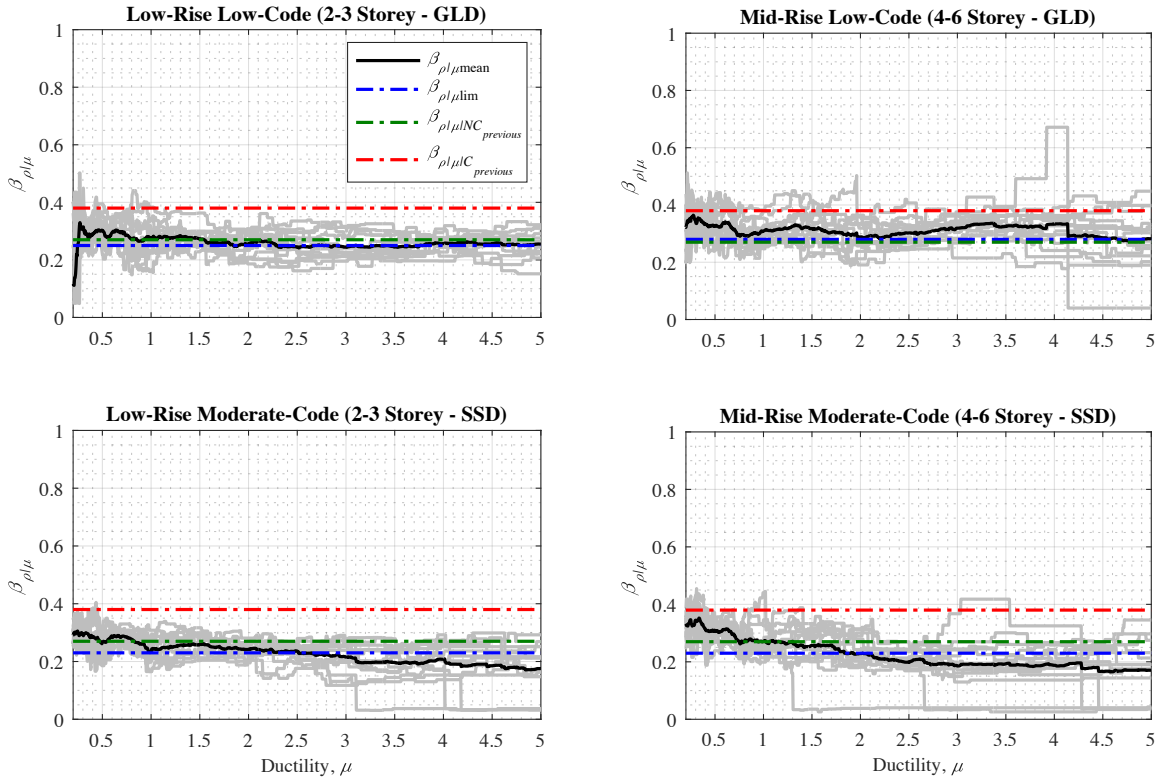

Figure 5: Trends in dispersion associated with the normalized strength ratio given ductility for low and mid-rise buildings designed for low and moderate code levels. The previously and newly suggested limits for fragility assessment are also illustrated.

Table 1: Newly derived dispersion limits to be integrated in parallel with the response estimation tool for the fragility function estimation of infilled RC frame buildings

Seismic code level	Number of Storeys	Taxonomy Code	Dispersion limit, $\beta_{\rho\|\mu}$
Low (GLD)	Low-Rise(2-3)	LC-LR	0.25
	Mid-Rise(4-6)	LC-MR	0.23
Moderate (SSD)	Low-Rise(2-3)	MC-LR	0.28
	Mid-Rise(4-6)	MC-MR	0.23

3 CASE STUDY EXAMPLE

A case study highlights the implementation of the newly derived uncertainty values in vulnerability and risk-based applications. Therefore, a demonstration of the PB-Risk [23] method for estimating seismic risk, which integrates a response estimation tool developed by the authors of this study for the characterisation of seismic vulnerability [24] is presented. The aim is to integrate the newly derived dispersion estimates within the aforementioned simplified procedure to compare the outcome in terms of fragility functions with MSA. To this end, a 3-storey RC school building with masonry infill fictitiously located in Napoli was selected to validate the new set of dispersion values. The school building, illustrated in Figure 6, was constructed in the 1960s before the introduction of seismic design provisions and has been previously examined by O'Reilly *et al.* [36].

Table 2: Summary of the case study modal properties and yield spectral acceleration in both principal directions

Floor No.	Mass, m_i [tonnes]	X-direction			Y-direction		
		First-mode shape, $\Phi_{i,1}$	Period, T_1 [s]	Yield Spectral Acceleration, Sa_y [g]	First-mode shape, $\Phi_{i,1}$	Period, T_1 [s]	Yield Spectral Acceleration, Sa_y [g]
Base	0	0.00	0.62	0.42	0.00	0.36	0.20
First	985	0.22			0.22		
Second	960	0.56			0.57		
Third	806	1.00			1.00		

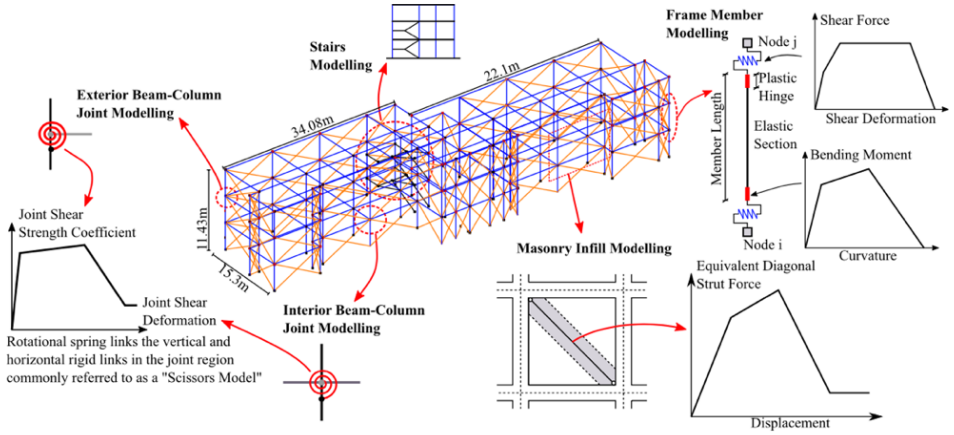

Figure 6: General layout and numerical modelling techniques of the case study school building. Adapted from O'Reilly et al. [36]

Concerning the simplified vulnerability-based assessment, the RET was applied. As such, SPO analyses characterizing the lateral load response of a case study building, expressed in terms of the base shear and roof displacement, are required in both principal direction (X and Y). Furthermore, SPO analyses were conducted using a displacement-controlled lateral load pattern proportional to the first-mode shape of the case study building. The SPO curves were then multi-linearised using the tool based on the onset and end of each response branch, namely: elastic, hardening, softening, residual plateau. Subsequently, dynamic capacity curves, expressed in terms of the median seismic intensity (i.e. Sa_{avg}) and roof displacement were empirically derived for both directions based on the multi-linearisation of the SPO results. Additionally, results from modal analyses (i.e. first-mode shape) are also necessary as inputs to retrieve the equivalent SDOF oscillator of an MDOF system to relate empirically the static and dynamic parameters. As such, eigenvalue analyses were performed whose results are reported in Table **2**. The results of the simplified vulnerability analyses using RET are presented in Figure 7 where the multi-linearised SPO curve and the dynamic capacity curves corresponding to the median, 16th and 84th fractiles are reported. The nominal base shear in both principal directions was normalized with respect to the yield nominal force of the structural system to obtain the static strength ratio ($\rho = V_b/V_{b,y}$) as highlighted in Figure 7. The ductility was derived by normalized the roof displacement with respect to the yield displacement ($\mu = {}^{\Delta}/_{\Delta_y}$). Figure 7 additionally demonstrates the dynamic capacity curve which were derived using the RET. These curves are expressed in terms of the dynamic strength ratio ($\rho = Sa_{avg}/Sa_y$) where Sa_y is the yield spectral acceleration. A dispersion $\beta_{\rho|\mu}$ value of 0.25 was used across the range of seismic response given that the case study school building belongs to the LC-LR taxonomy as reported in Table 1.

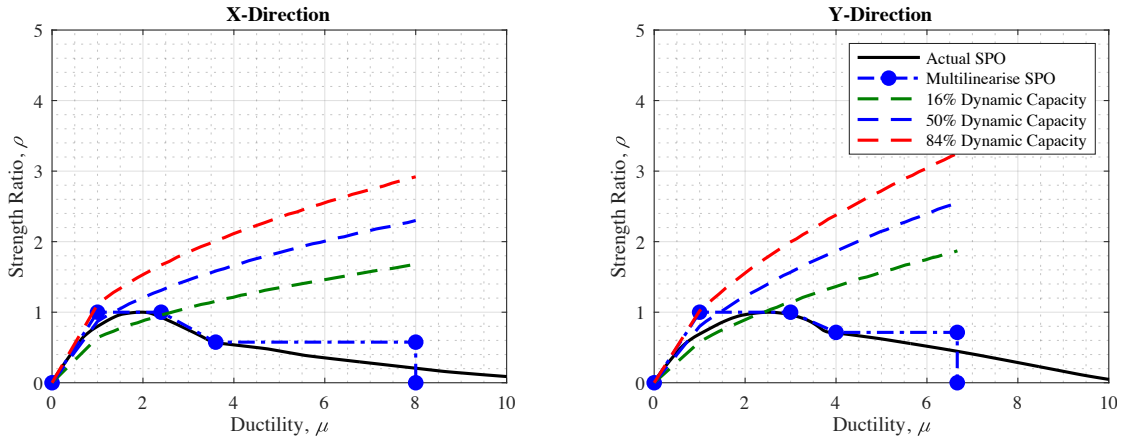

Figure 7: Results of the simplified seismic assessment carried out using the response evaluation tool in both principal directions

For what concern the extensive assessment, a series of MSA were carried out using hazard-consistent record sets selected in correspondence with the available hazard disaggregation at the conditioning period to evaluate the building response at increasing levels of intensity and return period. The conditioning period (T^*) was determined following modal analysis as the geometric mean of the fundamental periods in both principal direction ($T^* = T_{gm} = \sqrt{T_{1,x}T_{1,y}} = \sqrt{0.62 * 0.36} \approx 0.5$s). PSHA was carried out using the OpenQuake engine [32] considering Sa_{avg} as the IM. Records were then selected from the NGA database using the conditional mean spectrum method [37] with the modifications suggested by Kohrangi et al. [38] for Sa_{avg}. The correlation model by Baker and Jayaram [39] was used in all cases and the geometric mean of

the two components was used in the selection. Nine IM levels were investigated corresponding to a return period range of 22-4975 years for the characterization of the structural response covering initial damage of the masonry infill panels up to global structural collapse.

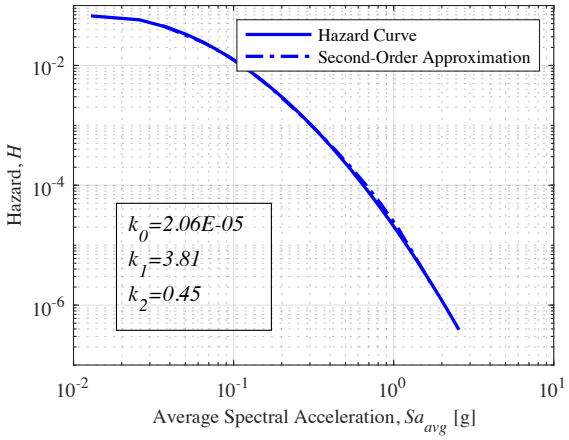

Figure 8: Hazard function obtained following PSHA expressing the hazard in terms of the annual rates of exceeding an intensity measure level and the second-order approximation required for the application of PB-Risk

The comparison between extensive and simplified assessment methods is illustrated via fragility functions where the median intensities and the associated dispersions obtained from both MSA and the response estimation method are reported. To this end, fragility functions of exceeding three arbitrary ductility thresholds are illustrated. These ductility thresholds correspond to the elastic limit ($\mu\approx1$), peak-capacity ($\mu\approx2$) and collapse ($\mu\approx5$). Scrutinizing the results of Figure **9**, it can be seen that for the X-direction, the response estimation tool has overestimated the median seismic intensities by almost double when compared with the results of NLTHA. However, MSA was carried out simultaneously along both principal directions of the three-dimensional buildings. Results have highlighted that the first instances of exceeding the arbitrary ductility thresholds have occurred in the Y-direction. Therefore, when assessing the performance of the response estimation tool for the Y-direction, it seems that the estimates provided by the tool were coherent with those reported using maximum likelihood estimation following MSA. The trends in fragility functions do not just highlight the robustness of the RET but also the accuracy in the newly derived dispersion values illustrated in the trends of the fragility functions. For the three arbitrary ductility thresholds selected, maximum likelihood estimation reported dispersions values of 0.28, 0.26 and 0.26 respectively, closely relevant with the suggested value for the case study taxonomy (LC-LR).

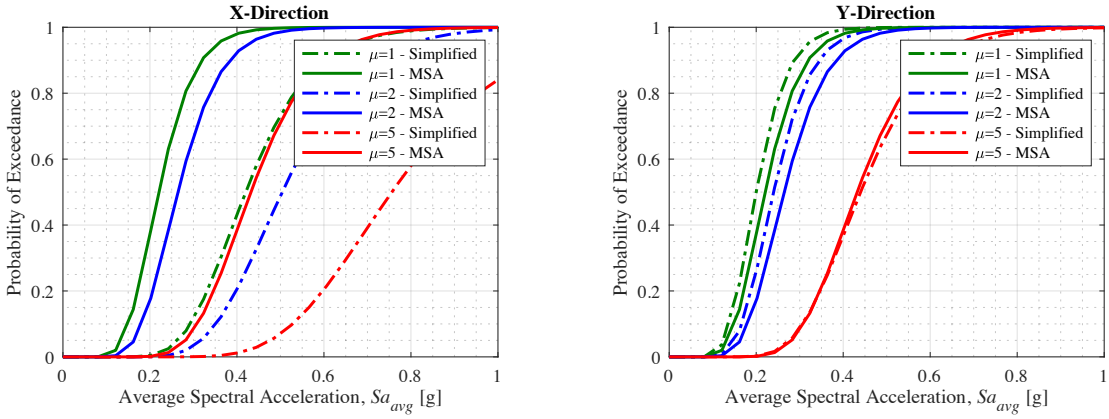

Figure 9: Fragility functions derived using MSA and RET for the arbitrary ductility threshold corresponding to the case study application

For the risk-based application, a comparison between simplified and extensive NLTHA was carried out. The former was done using the PB-Risk method [23] where the IM-based SAC/FEMA closed form solution (Equations 4 and 5) derived by Vamvatsikos [40] as an alternative to the classical risk integral (Equation 6) was integrated with the results of the RET (i.e median seismic intensities at demand-based thresholds and associated dispersions). As such, two main components are required for the calculation of the seismic risk in terms of the mean annual frequency of exceedance (MAFE or λ): (1) second-order coefficients following a robust mathematical fitting of the hazard function (Equation 3); (2) the resulting simplified vulnerability assessment parameters expressed in terms the median seismic intensity and the associated dispersions corresponding to exceeding a particular EDP threshold. To this end, first, a second-order fit of the hazard function was performed following Equation 3.

$$H(s) = k_0 \exp\left[-k_2 ln^2(s) - k_1 \ln(s)\right] \tag{3}$$

Where $H(s)$ is the hazard expressed in terms of the mean annual rate of exceeding an intensity measure level s; k_0, k_1 and k_2 are the resulting coefficients of the second-order fitting. The second-order fit and the coefficients of Equation 3 are illustrated and reported in Figure **8**.

For the application of PB-Risk, the second-order coefficients and the median seismic intensities and associated dispersions estimated from the RET corresponding to each ductility-based threshold were integrated in the closed-form solution provided in Equation 4. It is worth mentioning that for the implementation of PB-Risk, the results associated with the weaker direction were considered only. The results of the simplified risk assessment are reported in terms of MAFE in Table **3**.

$$\lambda = \sqrt{p} k_0^{1-p} [H(s)]^p \exp\left[\frac{k_1^2}{4k_2}(1-p)\right] \tag{4}$$

$$p = \frac{1}{1 + 2k_2\beta^2} \tag{5}$$

Utilising the results of extensive NLTHA analysis, a direct integration was carried out for the evaluation of the MAFE. Therefore, the median seismic intensities obtained following MSA and their associated dispersions were convolved with the hazard function at the chosen site for the derivation of the MAFE at the three considered ductility thresholds. This is performed following Equation 3. The results of the direct integration are reported in Table **3**.

$$\lambda = \int_0^{+\infty} P[\mu \geq \mu | IM = s] |dH(s)| \tag{6}$$

Comparing the results reported in Table **3** and subsequently the relative errors in Table **4** between the classical and simplified approaches presented here for the calculation of vulnerability and risk metrics, the benefits of an accurate quantification of uncertainty becomes further justified. This is especially true when shifting from vulnerability to risk as uncertainty propagates into the latter component. It can be seen that for both complexity levels in analysis, the choice of dispersion is of utmost importance. The PB-Risk methodology where the dispersion

limits established in this study were integrated highlighted an acceptable trade-off between accuracy and computational effort. A good agreement was concluded between the results of classical and simplified methodologies presented in this study.

Table 3: Summary of the simplified and extensive vulnerability and risk assessments

Vulnerability Assessment				
Ductility Thresholds	Response Estimation Tool		Multiple Stripe-Analysis	
	Median intensity, Sa_{avg} [g]	Dispersion, β	Median intensity, Sa_{avg} [g]	Dispersion, β
μ=1	0.20	0.25	0.22	0.28
μ=2	0.24		0.27	0.26
μ=5	0.44		0.43	0.26
Risk Assessment				
Ductility Thresholds	PB-Risk (Equation 4)		Direct Integration (Equation 6)	
	MAFE, λ			
μ=1	0.0031		0.0029	
μ=2	0.0021		0.0019	
μ=5	4.92E-04		5.02E-04	

Table 4: Calculated errors in the estimation of vulnerability and risk metrics
(*- underestimates; + overestimates)

Ductility Thresholds	**Vulnerability Assessment**		**Risk Assessment**
	Error in Median Intensity Estimation	Error in Dispersion Estimation	Error in MAFE Estimation
μ=1	9.09% (-)	10.71% (-)	6.89% (+)
μ=2	11.11% (-)	3.84% (-)	10.52% (+)
μ=5	2.32% (+)	3.84% (-)	1.6% (+)

4 CONCLUSIONS

Infilled reinforced concrete (RC) buildings represent a large portion of the southern Mediterranean built environment generally and the Italian building stock specifically. Therefore, the accurate seismic performance assessment of the infilled RC typology and its sub-taxonomies is of utmost importance for the earthquake engineering community. For vulnerability-based application, this is typically quantified using fragility curves which associate the probability of exceeding demand-based thresholds for given intensity measure levels. For risk-based application, the seismic performance is expressed in terms of the mean annual frequency of exceeding demand-based thresholds. In both applications, the proper characterization of the overall uncertainty and its subsequent reduction is an important asset. To this end, a simplified methodology denoted "PB-Risk" was presented in this study which allows for a simplistic characterization of vulnerability and risk components. Additionally, this study presented a calibration of epistemic uncertainty limits given sub-categories or taxonomies pertaining to the infilled RC typology (i.e. dispersion associated with record-to-record variability). The limits are presented and integrated within the PB-Risk methodology and subsequently compared to results of extensive nonlinear time-history analysis. The comparative case study application highlighted a good agreement between the results obtained via extensive or classical tools and the simplified approach presented in this study.

REFERENCES

1. Verdi VI a G, Cb AC, Famiglia FDI, Popolazione D, Abitazioni ED. Censimento generale della popolazione e delle abitazioni 2011: 1–24.

2. European Standard. Eurocode 8: Design of structures for earthquake resistance — Part 1: General rules, seismic actions and rules for buildings. *European Committee for Standardization* 2003.

3. NTC. *Norme Tecniche Per Le Costruzioni*. Rome, Italy: 2018.

4. Crowley H, Despotaki V, Silva V, Dabbeek J, Romão X, Pereira N, *et al.* Model of seismic design lateral force levels for the existing reinforced concrete European building stock. *Bulletin of Earthquake Engineering* 2021; **19**(7): 2839–2865. DOI: 10.1007/s10518-021-01083-3.

5. Fajfar P. Analysis in seismic provisions for buildings: Past, present and future. *Geotechnical, Geological and Earthquake Engineering*, vol. 46, 2018. DOI: 10.1007/978-3-319-75741-4_1.

6. Crowley H, Rodrigues D, Silva V, Despotaki V, Martins L, Romão X, *et al.* The European seismic risk model 2020 (ESRM20). *Proceedings of the International Conference on Natural Hazards and Infrastructure* 2019; **2020**(June 2019).

7. Romão X, Pereira N, Castro M, De Maio F, Crowley H, Silva V, *et al.* European Building Vulnerability Database v1.0 2020.

8. De Luca F, Woods GED, Galasso C, D'Ayala D. RC infilled building performance against the evidence of the 2016 EEFIT Central Italy post-earthquake reconnaissance mission: empirical fragilities and comparison with the FAST method. *Bulletin of Earthquake Engineering* 2018; **16**(7): 2943–2969. DOI: 10.1007/s10518-017-0289-1.

9. Parisi F, Luca F De, Petruzzelli F, Risi R De, Chioccarelli E. *Field inspection after the May 20th and 29th 2012 Emilia-Romagna earthquakes*. 2012.

10. Salvatore W, Caprilli S, Barberi V. *Rapporto dei Danni Provocati dall'Evento Sismico del 6 Aprile sugli Edifici Scolastici del Centro Storico dell'Aquila*. 2009.

11. MCEER. *The Marmara, Turkey Earthquake of August 17, 1999: Reconnaissance Report*. 2000.

12. O'Reilly GJ, Sullivan TJ. Modeling Techniques for the Seismic Assessment of the Existing Italian RC Frame Structures. *Journal of Earthquake Engineering* 2019; **23**(8): 1262–1296. DOI: 10.1080/13632469.2017.1360224.

13. O'Reilly GJ, Sullivan TJ. Probabilistic seismic assessment and retrofit considerations for Italian RC frame buildings. *Bulletin of Earthquake Engineering* 2018; **16**(3): 1447–1485. DOI: 10.1007/s10518-017-0257-9.

14. Fardis MN, Calvi GM. Effects of infills on the global response of reinforced concrete frames. *Proceedings on the 10th European Conference on Earthquake Engineering, Vienna*, Balkema, Rotterdam: 1994.

15. Dolšek M, Fajfar P. The effect of masonry infills on the seismic response of a four storey reinforced concrete frame-a probabilistic assessment. *Engineering Structures* 2008; **30**(11): 3186–3192. DOI: 10.1016/j.engstruct.2008.04.031.

16. Kurukulasuriya M, Milanesi R, Bolognini D, Lanese I, Grottoli L, Magenes G, *et al.* Shaking table experimental campaign on pre-code masonry infills subjected to in-plane and out-of- plane loading. *SPONSE*, Stanford, California: 2022.

17. Morandi P, Hak S, Milanesi RR, Magenes G. In-plane/out-of-plane interaction of strong masonry infills: From cyclic tests to out-of-plane verifications. *Earthquake Engineering*

& Structural Dynamics 2022; **51**(3): 648–672. DOI: 10.1002/eqe.3584.

18. Milanesi RR, Morandi P, Hak S, Magenes G. Experiment-based out-of-plane resistance of strong masonry infills for codified applications. *Engineering Structures* 2021; **242**: 112525. DOI: 10.1016/j.engstruct.2021.112525.
19. Morandi P, Hak S, Magenes G. In-plane experimental response of strong masonry infills. *9th International Masonry Conference*, Guimaraes, Portugal: 2014.
20. O'Reilly GJ, Nafeh AM., Shahnazaryan D. Simplified tools for the risk assessment and classification of existing buildings. *XIX ANIDIS Conference, Seismic Engineering in Italy*, Torino, Italy: 2022.
21. Nafeh AMB, O'Reilly GJ, Monteiro R. Simplified seismic assessment of infilled RC frame structures. *Bulletin of Earthquake Engineering* 2020; **18**(4): 1579–1611. DOI: 10.1007/s10518-019-00758-2.
22. Nafeh AM., O'Reilly GJ. Unbiased simplified seismic fragility estimation of non-ductile infilled RC structures. *Soil Dynamics and Earthquake Engineering* 2022; **157**: 107253. DOI: 10.1016/j.soildyn.2022.107253.
23. Nafeh AMB, O'Reilly GJ. Simplified pushover-based seismic risk assessment methodology for existing infilled frame structures. *Bulletin of Earthquake Engineering* 2023. DOI: 10.1007/s10518-022-01600-y.
24. Nafeh AMB, O'Reilly GJ. Unbiased simplified seismic fragility estimation of non-ductile infilled RC structures. *Soil Dynamics and Earthquake Engineering* 2022; **157**: 107253. DOI: 10.1016/j.soildyn.2022.107253.
25. O'Reilly GJ, Nafeh AMB. Infilled-RC-Building-Database. *GitHub Repository* 2021. DOI: 10.5281/zenodo.5082990.
26. F M, GL F, MH. S. OpenSees: open system for earthquake engineering simulation. *Pacific Earthquake Engineering Research Center, University of California, Berkeley* 2007.
27. Di Domenico M, Ricci P, Verderame GM. Empirical calibration of hysteretic parameters for modelling the seismic response of reinforced concrete columns with plain bars. *Engineering Structures* 2021; **237**: 112120. DOI: 10.1016/j.engstruct.2021.112120.
28. De Risi MT, Ricci P, Verderame GM. Modelling exterior unreinforced beam-column joints in seismic analysis of non-ductile RC frames. *Earthquake Engineering and Structural Dynamics* 2017; **46**(6): 899–923. DOI: 10.1002/eqe.2835.
29. De Risi MT, Verderame GM. Experimental assessment and numerical modelling of exterior non-conforming beam-column joints with plain bars. *Engineering Structures* 2017; **150**: 115–134. DOI: 10.1016/j.engstruct.2017.07.039.
30. Crisafulli FJ, Carr AJ, Park R. Analytical modelling of infilled frame structures - A general review. *Bulletin of the New Zealand Society for Earthquake Engineering* 2000; **33**(1): 30–47. DOI: 10.5459/bnzsee.33.1.30-47.
31. Hak S, Morandi P, Magenes G, Sullivan TJ. Damage control for clay masonry infills in the design of RC frame structures. *Journal of Earthquake Engineering* 2012; **16**(SUPPL. 1): 1–35. DOI: 10.1080/13632469.2012.670575.
32. Pagani M, Monelli D, Weatherill G, Danciu L, Crowley H, Silva V, *et al.* Openquake engine: An open hazard (and risk) software for the global earthquake model.

Seismological Research Letters 2014; **85**(3): 692–702. DOI: 10.1785/0220130087.

33. Eads L, Miranda E, Lignos DG. Average spectral acceleration as an intensity measure for collapse risk assessment. *Earthquake Engineering and Structural Dynamics* 2015; **44**(12): 2057–2073. DOI: 10.1002/eqe.2575.
34. Lin T, Haselton CB, Baker JW. Conditional spectrum-based ground motion selection. Part I: Hazard consistency for risk-based assessments. *Earthquake Engineering & Structural Dynamics* 2013; **42**(12): 1847–1865. DOI: 10.1002/eqe.2301.
35. Ozsarac V, Monteiro R, Calvi GM. Probabilistic seismic assessment of reinforced concrete bridges using simulated records. *Structure and Infrastructure Engineering* 2021: 1–21. DOI: 10.1080/15732479.2021.1956551.
36. O'Reilly GJ, Perrone D, Fox M, Monteiro R, Filiatrault A. Seismic assessment and loss estimation of existing school buildings in Italy. *Engineering Structures* 2018; **168**: 142–162. DOI: 10.1016/j.engstruct.2018.04.056.
37. Baker JW. Conditional Mean Spectrum: Tool for Ground-Motion Selection. *Journal of Structural Engineering* 2011; **137**(3): 322–331. DOI: 10.1061/(asce)st.1943-541x.0000215.
38. Kohrangi M, Bazzurro P, Vamvatsikos D, Spillatura A. Conditional spectrum-based ground motion record selection using average spectral acceleration. *Earthquake Engineering and Structural Dynamics* 2017; **46**(10): 1667–1685. DOI: 10.1002/eqe.2876.
39. Baker JW, Jayaram N. Correlation of spectral acceleration values from NGA ground motion models. *Earthquake Spectra* 2008; **24**(1): 299–317. DOI: 10.1193/1.2857544.
40. Vamvatsikos D. Derivation of new SAC/FEMA performance evaluation solutions with second-order hazard approximation. *Earthquake Engineering & Structural Dynamics* 2013; **42**(8): 1171–1188. DOI: 10.1002/eqe.2265.